

Design Study of Acceleration and Utilization of High-Power Beams in the RIA Facility[†]

P.N. Ostroumov, V.N. Aseev, J.A. Nolen

Physics Division, Argonne National Laboratory, 9700 S. Cass Avenue, Argonne, IL 60439, USA

Abstract. The Rare Isotope Accelerator (RIA) Facility currently being designed in the U.S. will use both heavy ion and light ion beams to produce radionuclides via the fragmentation and spallation reactions, respectively. A cw 1.4 GV driver linac is being developed for the RIA Facility. Because of the cw mode of operation, production of 400 kW light ion beams is straightforward and does not involve any technical challenges. However, acceleration of heavy ions, especially uranium, requires careful design and optimization of all systems of the driver linac. The linac is designed to accept and accelerate multiple charge state heavy ion beams, therefore, 100 kW uranium beam power could be available immediately. The further increase of uranium beam power will be achieved by appropriate ion-source development. The switchyard for the high-power beams of RIA will have the following features: 1) Distribution of various ion species accelerated to a wide range of energies to four target stations; 2) Delivery of beams to two target stations simultaneously; 3) Providing high quality beam optics with higher order corrections for multiple charge state beams to produce small beam spots at the entrance of the fragment separators. A rf sweeper is used for beam delivery to two targets simultaneously.

I. GENERAL LAYOUT OF THE RIA DRIVER LINAC

A conceptual design of the driver linac has been developed, the major elements of which are shown in Fig. 1. Except for the injector Radio Frequency Quadrupole (RFQ), the entire linac is based on superconducting (SC) accelerating structures, which not only enable cost-effective cw operation, but also, as discussed below, have numerous additional advantages for this application. The baseline design of the linac contains 9 types of SC accelerating cavities.

The layout, configuration, and many details of the RIA driver linac have been discussed and presented at several conferences and workshops [1-6]. Independent phasing of SRF cavities allows the velocity profile to

be varied: the linac can be tuned to provide higher energies for the lighter ions. For example, the reference design linac can be tuned to provide a uranium beam at an energy of 403 MeV/u and can be re-tuned to provide a proton beam at 900 MeV. To obtain 403 MeV/u uranium beams the driver linac uses two strippers. Three different sections of the linac are demarked by the charge-strippers. The low- β section of the linac is that portion prior to the first stripper, the medium- β section is that between the two strippers, and the high- β section is that portion following the second stripper. The low- β section includes a Front End with the possibility to accept for acceleration two-charge states simultaneously [7] and SC linac up to ~ 10.0 MeV/u for uranium. The medium- β and high- β section are designed for acceleration of multiple charge state beams. After each stripper there is a

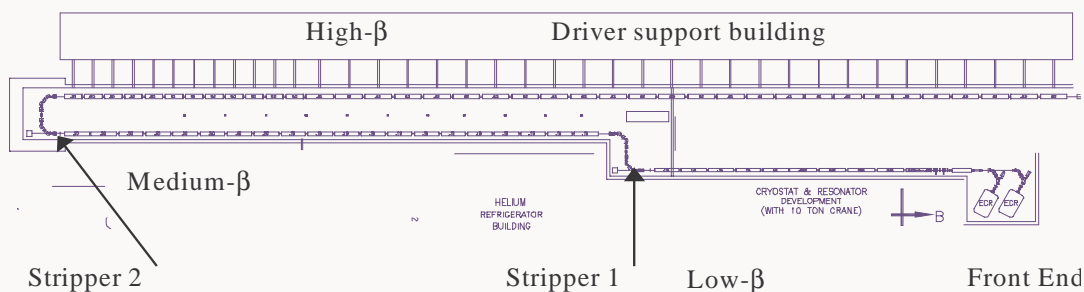


Figure 1. Elements of the proposed RIA driver linac.

[†] Work supported by the U. S. Department of Energy under contract W-31-109-ENG-38.

magnetic transport system which provides six-dimensional matching of multiple charge state beams to the following accelerating structure. In order to avoid beam losses in the high-energy section of the driver linac the low-intensity unwanted charge states must be carefully separated and dumped. This magnetic transport system requires focusing, dipole, and sextupole magnets and a rebuncher in order to provide a proper transformation of the 6-dimensional beam emittance.

Beam dynamics studies have been performed with the goal of optimization of the linac structure in order to reduce a possible effective emittance growth of the multi-q uranium beam. The dynamics of single- and multiple-charge state beams are detailed, including the effects of possible errors in rf field parameters and misalignments of transverse focussing elements. The end-to-end simulation of beam dynamics is being performed by the TRACK code [8] which integrates the particle equations of motion through the electric and magnetic fields of the superconducting cavities, the 3D field components having been obtained from numerical solution of Maxwell's equations for each specified cavity geometry. The motion of the particles is traced in 6D phase space, and generally represents the dynamics of the multi-component heavy-ion beams with good spatial resolution. After recent modifications the TRACK code supports all elements of the driver linac such as RFQ, multi-harmonic buncher, bending magnets, magnetic and electrostatic focusing devices. All TRACK elements are represented with realistic three-dimensional field distribution which naturally includes fringe fields. Initial first-order design of the linac is done by the TRACE code [9]. Beam transport codes such as TRANSPORT [10], GIOS [11] and COSY [12] were used for the design of multi-q beam transitions and switchyard. Comparative beam dynamics studies in the high- β section of the RIA driver linac have been performed for two types of accelerating structures: elliptical cavities as in the baseline proposal and triple-spoke cavities [5] which are being developed for intermediate beam velocity range $0.45 \leq \beta \leq 0.7$.

The longitudinal and transverse acceptance of the high- β section is ~ 100 times larger than the input beam emittance, which is determined by the ion source and injector RFQ. Such an immense margin for emittance growth makes possible a novel operating mode for the linac, in which the beam contains multiple charge-states [13, 14]. By simultaneously accelerating several of the multiple charge states resulting from stripping the beam, a much higher portion of the stripped beam can be utilized. The increase in efficiency not only provides a substantial increase in the available beam current, but also enables the use of multiple strippers, reducing the size of the

linac required for 400 MeV/u beams. A third benefit of using multiple charge states is a reduction in the amount of beam dumped during charge-state selection at the stripping points: this in turn reduces shielding requirements. It should be noted that the feasibility of multiple charge-state (multi-q) beam acceleration has been experimentally established in a series of tests with the existing SC ion accelerator ATLAS [15] operated at Argonne National Laboratory. In addition, it was shown that the Front End of the driver linac can be designed for the acceptance of two charge states of uranium beam from the Electron Cyclotron Resonance (ECR) ion source, doubling the available uranium beam power [16].

The driver linac is a high intensity machine and relative beam losses in the high-energy section must be kept below 10^{-4} . Acceleration of multi-q uranium beam places stringent requirements on the linac design. Any other lighter ion beams can be accelerated with much smaller emittances. End-to-end beam dynamics simulations in six-dimensional phase space have been applied to study all possible sources of beam halo formation and possible beam loss in the driver linac. Major contributors to the effective emittance growth are identified and they are: a) multiplicity of charge states; b) passage through the stripping foils and c) random errors of rf fields and misalignments of focusing elements. We have developed the concept of a "beam-loss-free" linac which implies beam halo collimation in designated areas.

II. FRONT END OF THE DRIVER LINAC

The front end of the RIA driver linac is shown schematically in Fig. 2. It consists of two ECR ion sources, a low energy beam transport (LEBT), a multi-harmonic buncher, a 57.5 MHz RFQ, and, finally, a medium energy beam transport (MEBT) which matches beam into the superconducting linac.

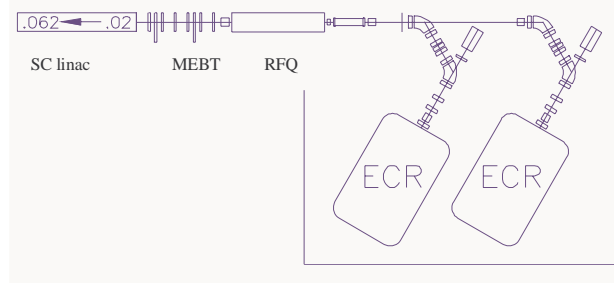


Figure 2. Front End of the RIA driver linac.

An ECR type of source is well matched to the requirement for cw, high-charge-state ion beams over the full mass range. The heaviest beam needed for the

RIA driver is uranium, which is the most demanding in terms of ion source performance. Current state-of-the-art ECR sources, such as the ECR at Berkeley [17], can probably provide sufficient beam to produce more than 100 kW of output beam in two charge states. The LEBT is designed to select and separate the required ion species and to bunch and match either one or two charge states into the following RFQ structure. The first portion of the LEBT is an achromatic bending-magnet section for charge-to-mass analysis and selection. For the heaviest ions with masses above 180, the transport system is capable of delivering to the entrance of the first buncher a two-charge-state beam with similar Twiss parameters for both charge states. In order to match two-charge-state ions with masses different from uranium, the straight section of the LEBT upstream of the RFQ will be placed on high-voltage platform. A voltage ~ 30 kV is required in order to match velocities of ions in mass range $180 \leq A \leq 238$ and maintain the possibility to accelerate two charge states simultaneously. The ECR is placed on a high voltage (HV) platform. The voltage should be higher than 100 kV to avoid space charge effects in the LEBT for 400 kW accelerated beams. Currently the required voltage of the ECR HV platform is being studied using the criteria of lowest emittance growth of the high-intensity two-charge-state beam along the achromatic bend.

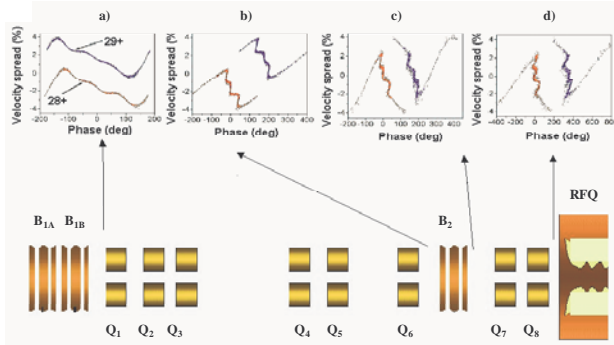


Figure 3. Layout of the LEBT and longitudinal phase space plots of a two-charge state beam along the LEBT: a) after B_1 , b) before B_2 , c) after B_2 , d) RFQ entrance with scale changed to RFQ frequency.

A simplified layout of the second part of the LEBT is shown in Fig. 3. This part of the LEBT solves the following tasks: a) Beam bunching by a four-harmonic external buncher B_1 (the fundamental frequency is 28.75 MHz); b) Velocity equalization of two different charge states by the buncher B_2 , operating at 28.75 MHz; c) Charge-insensitive transverse focusing of the 2-charge state beam and matching to the RFQ acceptance by the electrostatic quadrupoles Q_1 - Q_8 . The LEBT, RFQ and MEBT have

been designed using numerical modeling with full 3-D field approximations. The reference beam is uranium at a average charge state of 28.5. Note that the system will, however, accelerate any beam from uranium to protons to a velocity $v/c = 0.02$ at the exit of the RFQ. The design assumes a normalized total transverse emittance of 0.5π mm-mrad. The voltages of the multi-harmonic buncher have been optimised, together with the RFQ parameters, in order to obtain a total efficiency above 80%, while minimizing the longitudinal emittance for each charge state. The second buncher is used to equalize the velocities of the 2 charge states (see Fig. 3c). The primary design goal for the RFQ is to establish a low output emittance so that the acceleration of multiple-charge-state beams through the rest of the linac becomes straightforward. As was discussed in our previous work [15], a multi-harmonic buncher must be used upstream of the RFQ to produce the lowest possible longitudinal emittance of two charge state beams. The acceleration starts with a small separatrix whose length is kept constant along the RFQ. For the parameters of the RFQ given in ref. [17] the longitudinal emittance at the level 99.9% is less than 2π keV/u-nsec for a two-charge state uranium beam. This number was obtained from simulation of the $5 \cdot 10^4$ particles with initial transverse emittance 0.5π mm-mrad.

The MEBT system must transport and match the full 6-dimensional phase-space for a two-charge state beam from the RFQ into the SC drift-tube linac. The following components are required to accomplish this task:

- 1) Transverse focussing elements.
- 2) Rebunchers.
- 3) Beam diagnostics tools.
- 4) Steering magnets for simultaneous correction of centroids of the two-charge state beam.

At the beginning of the MEBT, the transverse phase-space canonical ellipses coming out of the RFQ are matched into an axially-symmetric channel by three strong magnetic quadrupole singlets. An option to extract axially-symmetric beams directly from the RFQ is being studied. A major design problem in the remainder of the MEBT is to provide transverse focussing without introducing additional mismatch between the different charge states for the two-charge-state beams. We have considered several options, quad doublets, quad triplets, and solenoid focussing. Solenoid focussing proved to introduce the least mismatch of two-charge state beams through the rest of the MEBT.

III. SUPERCONDUCTING LINAC

Much of the driver linac is based on the well-

established technology employed in currently operating SC rf accelerators. These machines fall into two classes. The first class consists of electron linacs for velocities $\beta > 0.9$, which employ relatively high-frequency SC niobium elliptical-cell cavities operating near 2 K. The second class consists of heavy-ion linacs providing ions at velocities $0.01 < \beta < 0.2$, which employ relatively low-frequency SC drift-tube structures operating near 4 K. Recent development work is extending the velocity range of SC rf structures to cover the full velocity range required by the RIA driver. This is being accomplished by developing foreshortened elliptical-cell-type structures down to $\beta = 0.49$, and various drift-tube type structures for velocities up to $\beta = 0.5$ [5].

III.A. Accelerating-Focusing Lattice

The baseline design of the driver linac was described in ref. [6]. Below we present a variation of the baseline design which includes the following main modifications: 1) peak surface electric field in all drift-tube SC resonators assumed to be 20 MV/m except first seven 4-gap ‘‘ATLAS type’’ resonators; 2) the high- β section of the driver linac contains two types of triple-spoke resonators (TSR) instead of three types of elliptical resonators operating at a peak electric field 27.5 MV/m [5]. Overall, in this variation of the baseline design there are only seven types of SC resonators versus nine types in the baseline design.

Except the first cryostat which contains seven 4-gap resonators and one 2-gap resonator, the linac

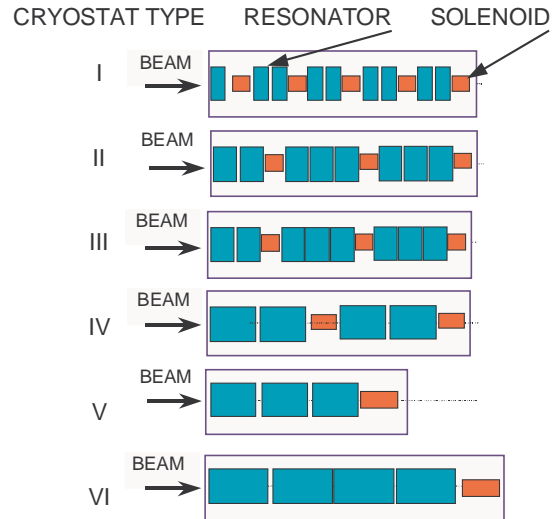


Figure 4. Layout of 6 different types of cryostats along the driver linac (not to scale).

consists of 6 different types of cryostats filled by five different types of resonators as is seen from Fig. 4. The main parameters of the accelerating-focusing lattice are given in Table 1. The linac comprises 352 SC cavities distributed in 68 cryostat modules. Table 1 does not show the first cryostat which consists of seven 4-gap quarter-wave resonators (QWR). Transverse focussing is provided by SC solenoids contained in the same cryostat modules as the cavities. Such an array, with the cavities operated at a synchronous phase $\phi_s = -30^\circ$, provides strong focussing

Table I. Basic parameters of the lattice.

Cryostat type as is shown in Fig. 6	I	II	III	IV	V	VI
Frequency (MHz)	57.5	115	172.5	345	345	345
Cavity beta	0.061	0.15	0.252	0.50	0.50	0.62
Number of cryostats	4	5	12	8	12	26
Number of cavities	37*	41 [†]	96	33 [†]	36	104
Length of focusing period (m)	1.13	1.77	1.73	2.38	3.98	5.80
Number of cavities per focusing period	2	3	3	2	3	4
Beam energy (MeV/u)	4.78	10.15	55.33	86.3	148.3	402.15
Aperture diameter (mm)	30	30	30	40	40	40
Synchronous phase (deg)	-30	-25	-30	-30	-30	-25
ype of cavity	QWR	QWR	HWR	TSR	TSR	TSR
Peak surface field (MV/m)	20	20	20	28	28	28
Accelerating field (MV/m)	5.71	5.41	6.45	8.45	8.45	8.45
Eff. length of the SC solenoids (cm)	18	30	30	30	40	50
Focusing field of the SC solenoids (T)	6.6-9.2	8.3-11.0	5.8-8.6	8.6-9.5	6.8-9.0	8.7
RMS misalignments of the ends of the solenoid (mm)	0.17					
Random rms fluctuation of RF field phase (deg)	0.3					
Random rms fluctuation of the field amplitude (%)	0.3					

*Includes one cavity located in the first cryostat.

[†]Including a cavity-rebuncher.

in both transverse and longitudinal phase space. Due to the strong damping of the bunch phase width as beam energy is increased the 115 MHz SRF cavities can be set at a synchronous $\phi_s = -25^\circ$. Prior to numerical ray-tracing a two charge-state beam was matched carefully using fitting codes for a trial beam. A particularly critical aspect of fitting was to avoid beam mismatch the transitions between focusing periods of differing length and between the cryostats. Note that the focusing lattice length is different for each type of SC cavities. Final adjustment of the longitudinal matching is done by setting appropriate value of synchronous phase. The focusing period of the first three types of cryostats contains two or three cavities per period except for the first period which forms a focusing period with a “missing” cavity. The space of the missed cavity is replaced by the inter-cryostat drift. The flange-to-flange distance between the elements located in adjacent cryostats is set to be 50 cm. The focusing structure with the “missing” cavity is extremely helpful for tuning of beam motion in the transverse phase space. A little adjustment of the focusing fields in outermost solenoids is required in order to match beam. Similar focusing structure is designed for the cryostats containing 115 MHz and 172.5 MHz SC cavities. Cryostats IV and V contain one type of TSR with geometrical beta $\beta_G = 0.5$ while cryostats VI consists of a second type of TSR with $\beta_G = 0.6$

III.B. Stripper Sections

The driver linac requires two charge-stripping sections. The passage of high intensity heavy ion beam through the stripping film, or foil, results in several effects:

- At the exit of the stripping foil, the ion beam is a mixture of several charge states, the intensities of which are a Gaussian distribution.
- The stripping foil experiences high thermal load, especially at the first stripper. A liquid lithium film for the first stripper is under development [18], both to accommodate the thermal load, and also to produce higher charge states.
- The average energy of the ion beam is slightly decreased due to ionisation losses in the stripper.
- The transverse and longitudinal beam emittances are increased due to the energy straggling and scattering.

Table 2 shows the effect of the stripper on the uranium beam. The beam scattering and energy straggling were calculated by the help of SRIM code [20]. However, the calculations in the RIA stripper energy range are not reliable. Currently we are working on experiments to understand the stripper effects on uranium beams at 10 MeV/u and 85 MeV/u.

Table 2: Stripper effect on uranium beam.

Beam energy (MeV/u)	10.3	86.0
Medium	Li	Li
Thickness (mg/cm^2)	0.2	15
Energy loss (MeV/u)	0.02	3.29
Mean charge state	72	89
Charge states	70-74	88-91
Beam fraction within design charge states (%)	69	96
Rms angle of transverse beam scattering (mrad)	0.2	0.5
Rms energy spread (keV/u)	4.0	18

The first experiments at 10 MeV/u show larger beam straggling than it is predicted by the SRIM code. This effect may be due to stripper foil non-uniformity.

In order to avoid beam losses in the high-energy section of the driver linac the low-intensity unwanted charge states must be carefully separated and dumped. As long as the driver linac is designed for acceleration of multi-q beams, the beam transport system following the stripping foil must provide simultaneous matching of selected charge states to six-dimensional acceptance of the following SRF linac [21]. This magnetic transport system (MTS) requires dipole magnets and a rebuncher in order to provide a proper transformation of the 6-dimensional beam emittance. The system has a dispersive area, effectively operating as a spectrometer. In the region of maximum dispersion, the unwanted charge states are removed by horizontal beam collimation. The beam matrix of the second moments must be the same at the entrance and exit of the system. The reproduction of the second order moments of the beam in the longitudinal phase space is provided for by the rf cavity which must be located in a zero dispersion area. All bunches of different charge state must arrive at the rf cavity at the same time (at the same phase of the rf field). This means that the MTS must have the same path length for all charge states in the initial portion, up to the rebuncher, and also, separately, in the output portion from the re-buncher on. At the final stage of the MTS design, the higher order terms were included and corrected as necessary.

We have designed such systems for both stripping areas. Several options for the MTS design can satisfy the above requirements. The options chosen seem to best satisfy the overall architectural requirements of the linac. For example, after the first stripper, it is convenient to transversely shift the linac beam axis: the MTS incorporates two 90° bends to provide a 7.2 m shift. After the second stripper it is economical to bend the beam through 180° , since such a bend greatly shortens the overall length of the linac tunnel (see Fig. 1). The 180° bend provides for high-dispersion regions

in the MTS which enable separation of low intensity charge states and cleaning or scraping of any beam halo in the transverse phase space. In this MTS configuration the beam collimation area will be well isolated from the clean, radiation-free accelerator systems.

III.C. Beam Dynamics Simulations

Beam dynamics in the SRF linac were numerically simulated using the TRACK code. The simulation starts from the exit of ECR HV platform. A multi-component heavy-ion beam is transported through the achromatic charge-selection system and accelerated by the RFQ. For 400 kW driver beams space charge effects are significant in the LEBT and have been included up to the end of the RFQ. In these simulations 10^6 particles remaining after the RFQ represent a two-charge state uranium beam in the low- β section, five charge states in the medium- β and four charge states in the high- β section. The beam envelope in the horizontal plane along the SC section of the linac is shown in Fig. 5. The beam is axially-symmetric along the linac but not in the post-stripper MTS. The passage through the strippers was simulated by the SRIM code [19] and the particle distribution was incorporated into TRACK. In the beam dynamics simulations for the safety margin we assumed that the standard deviation of the energy straggling is 5 times larger than the value predicted by the SRIM code. Table 3 shows the emittance growth in the linac with and without errors.

Table 3. Rms and total (100% of particles) emittance growth ratio in the driver linac

No errors			
	Horizontal	Vertical	Longitudinal
Rms	1.5	1.5	4.9
Total	4.8	4.9	35
With errors			
Rms	1.8	1.9	9.5
Total	5.8	6.8	35

All errors are randomly generated as a uniform distribution with the rms values listed in Table 1. The sensitivity of multi-q beam parameters to various types of random errors and misalignments were studied by the ray-tracing code TRACK. The most important errors affecting transverse beam motion are the misalignments of the transverse focusing elements. Due to the strong defocusing of low velocity particles by the SRF cavities the misalignments of the SRF cavities were taken into account too. Phase and amplitude errors of the rf field are fast fluctuations and produce effective longitudinal emittance growth of

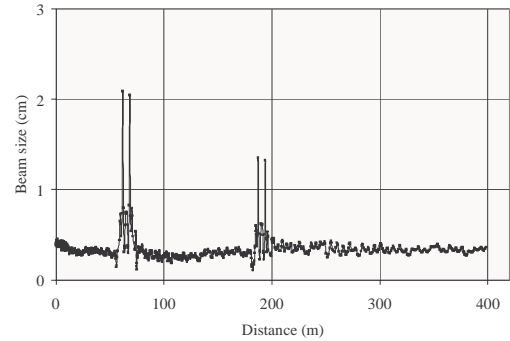


Figure 5. Beam maximum size in the horizontal plane along the driver linac.

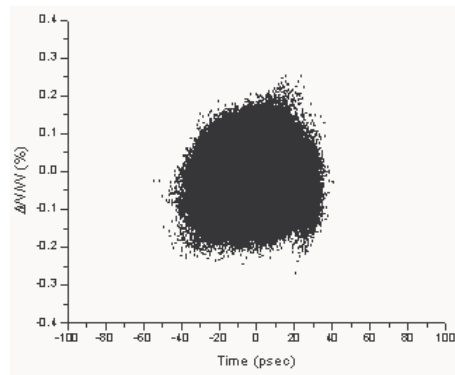


Figure 6. Phase space plots of a four charge state uranium beam at the exit of the driver linac. multi-q beams.

Monte Carlo simulations of the dynamics of multi-q beams in the presence of both accelerating field and alignment errors have been performed. We introduced alignment errors by displacing separately both ends of each solenoid and SRF cavity in both X and Y by an amount in accordance with the displacement values given Table 1. Then we tracked the multi-q beam represented by 5000 particles through the whole linac and noted the increase in emittance resulting from all types of errors. As was discussed in ref. [6] a multi-q beam requires frequent corrective steering in order to avoid appreciable emittance growth. Therefore our simulation was done in the presence of steering elements along the linac. This entire simulation was then repeated two hundred times, each time with a different, random set of errors. These studies show that in the case both transverse and longitudinal total emittances are well within the linac acceptance. No particle losses along the linac were observed.

Phase space plots obtained during 200 seeds are accumulated and shown in Fig. 6. As is seen the multi-q uranium beam can be accelerated up to 400 MeV/u within $\pm 0.25\%$ energy spread and remains within ± 40 picoseconds width. Longitudinal emittance of 80

π -keV/u-nsec contains all particles shown in Fig. 6.

IV. DESIGN OF THE RIA DRIVER LINAC SWITCHYARD

A preliminary design for a driver linac switchyard has been completed as is shown in Fig. 7. The switchyard delivers beams to four production targets. Driver beam power of up to 400 kW will be available so that beam sharing between target stations is desirable. Design of the switchyard for the driver beams of RIA is a unique task due to the following features: 1) Distribution of various ion species accelerated over a wide range of energies to four target stations; 2) Delivery of beams to two target stations simultaneously; 3) Providing high quality beam optics with higher order corrections for multiple charge state beams to produce small beam spots at the entrance of the fragment separators.

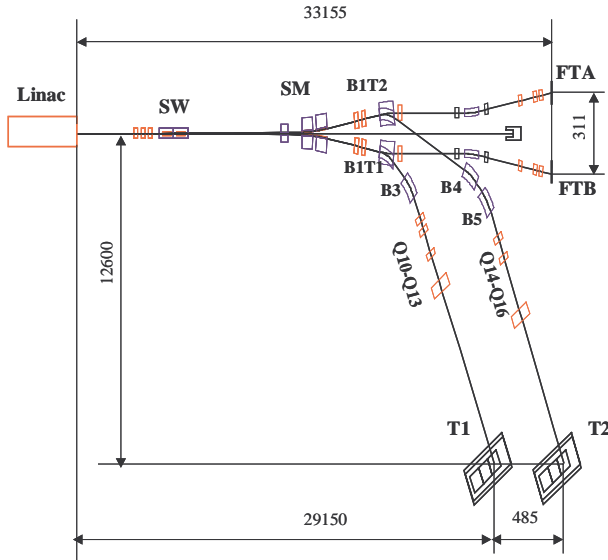


Figure 7. Layout of the driver linac switchyard. The distances are shown in mm. Legend: SW – rf sweeper; SM – septum magnets; B1T1, B1T2, B3, B4, B5 – bending magnets; Q10-Q13, Q14-Q16 – quadrupoles; FTA, FTB – fragmentation targets; T1, T2 – ISOL targets.

A low frequency rf sweeper is appropriate for deflection of heavy ion beams and for delivery to two or more targets simultaneously. The deflector design can be based on an H-type rf cavity. The fundamental frequency of the bunch sequence is determined by the multiharmonic buncher at the Front End of the driver linac. In the two-charge state injector mode all four harmonics are applied and bunch repetition rate will be 57.5 MHz. In the single charge state injector mode only three harmonics of the multi-harmonic buncher

will be used and bunch repetition rate is still 57.5 MHz. Therefore the rf sweeper can operate at 86.25 MHz to split the beam intensity 50/50 to two directions. The length of the electrode is chosen to provide phase slippage 180° inside the cavity for uranium beams. This condition eliminates any effect of fringing fields on uranium beams but produces negligible momentum spread for lighter ions because of higher velocity and shorter time-of-flight of lighter ion beams. A room temperature rf cavity operating at 86.25 MHz can provide a maximum electric field on the surface ~ 20 MV/m in cw mode. We have conservatively designed for a maximum electric field ~ 6 MV/m between the electrodes. The main parameters of the rf sweeper are shown in Table 4. Two such sweepers are used in series.

The rf sweeper is followed by two DC septum magnets. Beam envelopes of a four charge state uranium beam in the transport system from the linac exit to the fragmentation targets are shown in Fig. 8. The multi-q uranium beam is focused to a spot $X \times Y = 1.0 \times 3.0$ mm² in this example.

Table 4: Basic parameters of the rf deflector for the RIA switchyard

Maximum electric field	6 MV/m
Effective length	1.3 m
Deflecting angle	± 2 mrad
Characteristic resistance according the MAFIA simulations	3 Mohm
Required rf power (twice of MAFIA prediction)	11 kW

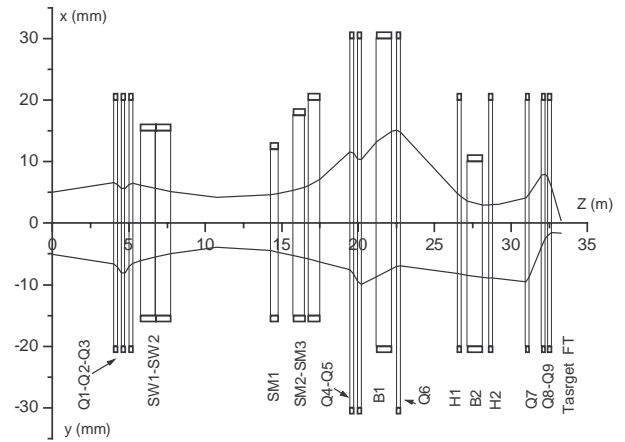


Figure 8. Multi-q uranium beam envelopes along the beamline from the linac to fragmentation separator targets FTA and FTB.

V. CONCLUSION

Preliminary design of the RIA driver linac and switchyard is completed. Several novel features have been implemented into the baseline design. Detailed end-to-end beam dynamics simulation has been performed for multi-q uranium beams from the ion source to the production targets. These simulations have been iterated repeatedly with the design of overall linac architecture. The simulations, which include misalignments of focusing and accelerating elements and random errors of the rf fields, show that beam emittances are well below the six-dimensional acceptance throughout of the whole SC linac. The concept of a “beam-loss-free” linac was developed and implies beam halo collimation in designated areas. By proper collimation along the post-stripper magnetic transport system, beam losses in the high-energy part of the accelerator can be avoided completely.

VI. REFERENCES

1. K. W. SHEPARD, J.R. DELAYEN, C.M. LYNEIS, J.A. NOLEN, P.N. OSTROUMOV, J.W. STAPLES, J. BRAELEY, C. HOVATER, M. KEDZIE, M.P. KELLY, J. MAMMOSSER, C. PILLER and M. PORTILLO, in the *Proceedings of the 9th International Workshop on RF Superconductivity, Santa Fe, New Mexico, 1999*, edited by B. Rusnak, p.345.
2. P.N. OSTROUMOV, K. W. SHEPARD, J.A. NOLEN, R.C. PARDO, in *ICFA Beam Dynamics Newsletter, No. 20, August, 1999*, p. 60.
3. C.W. LEEMANN, in *Proceedings of the 2000 Linac Conference, Monterey, California, August 21-25, 2000, SLAC -R-561*, edited by A.W. Chao, p.331.
4. J.A. NOLEN. *Proceedings of the XXI Int. Linac Conf., Gyeongju, Korea, August 19-23, 2002*, <http://linac2002.postech.ac.kr/db/proceeding/MO302.pdf>
5. K. W. SHEPARD. *Proceedings of the XXI Int. Linac Conf., Gyeongju, Korea, August 19-23, 2002*, <http://linac2002.postech.ac.kr/db/proceeding/TH301.pdf>
6. P. N. OSTROUMOV. *Phys. Rev. ST. Accel. Beams* **5**, 030101 (2002).
7. P.N. OSTROUMOV and K. W. SHEPARD, *Phys. Rev. ST Accel. Beams* **3**, 030101 (2000).
8. P. N. OSTROUMOV and K. W. SHEPARD, *Phys. Rev. ST. Accel. Beams* **11**, 030101 (2001).
9. K.R. CRANDALL. Report LA-11054-MS. Los Alamos, 1987.
10. K. L. BROWN, The ion optical program TRANSPORT. Technical Report 91, SLAC, 1979.
11. H. WOLLNIK, J. BREZINA and M. BERZ, *NIM, A258*, (1987) 408.
12. M. BERZ, COSY INFINITY, Version 8 User’s Guide and Reference Manual, MSU, 1999.
13. P.N. OSTROUMOV, J.A. NOLEN and K. W. SHEPARD, in *Proceedings of the 2000 Linac Conference, Monterey, California, August 21-25, 2000, SLAC -R-561*, edited by A.W. Chao, p.1018.
14. P.N. OSTROUMOV, R.C. PARDO, G.P. ZINKANN, K. W. SHEPARD and J.A. NOLEN, *Physical Review Letters*, **86**, N 13, 26 March 2001, p. 2798-2801 (2001).
15. P.N. OSTROUMOV, V.N. ASEEV, A.A. KOLOMIETS and K. W. SHEPARD, in *Proceedings of the 2000 Linac Conference, Monterey, California, August 21-25, 2000, SLAC -R-561*, edited by A.W. Chao, p. 202.
16. M.A. LEITNER, D.C. WUTTE and C.M. LYNEIS, in *Proceedings of the 2001 Particle Accelerator Conference, June 18-22, Chicago, IL, 2001*, p. 67.
17. P.N. OSTROUMOV, A.A. KOLOMIETS, D.A. KASHINSKY, S.A. MINAEV, V.I. PERSHIN, T.E. TRETYAKOVA, S.G. YARAMISHEV. *Phys. Rev. ST Accel. Beams* **5**, 060101 (2002).
18. J. NOLEN, C.B. REED, A. HASSANEIN, M. PORTILLO and J.H. NOREM, in *Physics Division Annual Report 2000, ANL-01/19, ANL, Argonne, IL, 2001*, p. 152.
19. J.F. ZIEGLER, J.P. BIRSACK and U. LITTMARK, *The Stopping and Range of Ions and Solids*, Pergamon Press, NY, 1996.
20. M. PORTILLO, V.N. ASEEV, J.A. NOLEN and P.N. OSTROUMOV, in *Proceedings of the 2001 Particle Accelerator Conference, June 18-22, Chicago, IL, 2001*, p. 3012.